Silver nanoparticles and wheat roots: a complex interplay

Ana Elena Pradas del Real, Vladimir Vidal, Marie Carrière, Hiram A. Castillo-Michel, Clement Levard, Perrine Chaurand, Géraldine Sarret

▶ To cite this version:

HAL Id: hal-01516961

https://hal.archives-ouvertes.fr/hal-01516961

Submitted on 11 May 2018

1   **Ag nanoparticles and wheat roots: a complex interplay**

2   Ana.E Pradas del Real[1,5*], Vladimir Vidal[2], Marie Carrière[3,4,] Hiram Castillo-Michel[5], Clément Levard[2],

3   Perrine Chaurand[2], Géraldine Sarret[1]

4   [1]ISTerre (Institut des Sciences de la Terre), Université Grenoble Alpes, CNRS, Grenoble, France.

5   [2] Aix-Marseille Université, CNRS, IRD, CEREGE UM34, 13545, Aix en Provence, France
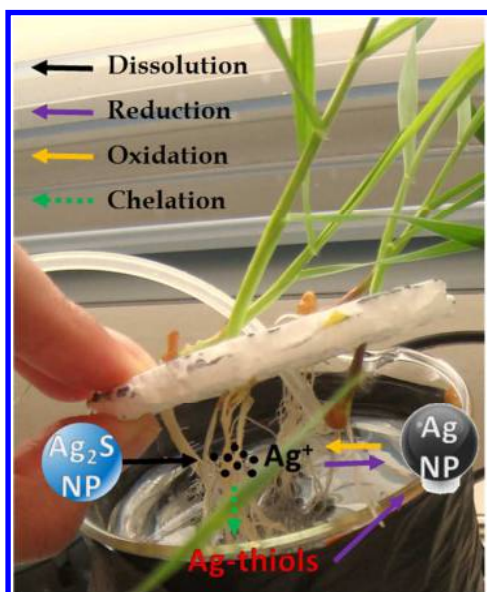
6   [3]Univ. Grenoble-Alpes, INAC-SCIB, F-38000 Grenoble, France

7   [4]CEA, INAC-SCIB, F-38000 Grenoble, France

8   [5] ID21, ESRF-The European Synchrotron, CS40220, 38043 Grenoble Cedex 9, France

9   *ana.pradas@univ-grenoble-alpes.fr, ana-elena.pradas@esrf.fr

10

11

12

13

14   **Graphical Abstract (TOC)**

15
16
17
18   **ABSTRACT**

19   Agricultural soils are major sinks of silver nanoparticles in the environment, and crops are directly

20   exposed to these emerging contaminants. A clear picture of their chemical transformations, uptake

21   and transport mechanisms, and phytotoxic impacts is still lacking. In this work, wheat plants were

22   exposed to pristine metallic (Ag-NPs) and sulfidized (Ag$_2$S-NPs) silver nanoparticles and ionic Ag. Data

23   on Ag distribution and speciation, phytotoxicity markers and gene expression were studied. A multi-

24   technique and multi-scale approach was applied combining innovating tools at both laboratory and

25   synchrotron. Various chemical transformations were observed on the epidermis and inside roots,

2

26   even for Ag_2S-NPs, leading to an exposure to multiple Ag forms, which likely evolve over time. Genes

27   involved in various functions including oxidative stress, defense against pathogens and metal

28   homeostasis were impacted in different ways depending on the Ag source. This study illustrates the

29   complexity of the toxicity pattern for plants exposed to Ag-NPs, the necessity of monitoring several

30   markers to accurately evaluate the toxicity, and the interest of interpreting the toxicity pattern in

31   light of the distribution and speciation of Ag.

32

33

34

35   **1. INTRODUCTION**

36   Agricultural soils are pointed as a major sink for engineered nanoparticles (NPs) due to the

37   application of sewage sludge[1], which contains various types of engineered nanomaterials (ENMS) and

38   their secondary products[2]. Current regulations concerning sewage sludge application focus on their

39   content of certain metals, none of them consider ENMS. The use of nanopesticides creates another,

40   not precisely quantified, input of NPs in soils[3]. Silver nanoparticles (Ag-NPs) are one of the most

41   prevalent metallic nanoparticles in consumer products due to their biocidal action[4]. Sulfidation is a

42   major transformation of Ag-NPs that starts during the use of the products (e.g., laundry washing for

43   textiles)[2] and is completed during wastewater treatment[3], making silver sulfide (Ag_2S) the main Ag-

44   species in sewage sludge[5]. Due to the extremely low solubility of microcrystalline Ag_2S, sulfidation

45   has been considered as a natural antidote against Ag-NPs toxicity[6] . This opinion requires refinement

46   since in sludges and soils Ag_2S precipitate in presence of other compounds (mostly organics)

47   potentially forming nanometric and multiphasic Ag-S forms whose solubility is not known[2].

48   Moreover, a recent study evidenced the dissolution of Ag_2S NPs in aquatic media[7].

49   Contrarily to other metals, natural Ag enrichments in soils are rare[8], so there is no known plant

50   species, which has evolved to cope with Ag toxicity. The toxicity of Ag-NPs is supposed to be primarily

51   due to the release of Ag+ ions. Besides this, it could be a toxicity related with the characteristics of

52   the nanoparticles (size, specific surface area, surface charge) that are not exerted by the bulk Ag.[9-11]

53   As for other ENMs, the transfer of Ag-NPs inside plant tissues has been observed[9,12], but it is difficult

54   to conclude on their direct transfer since it could result from Ag^+ reduction inside plants. Various

55   toxicity symptoms and up-regulation of genes linked with oxidative stress have been observed[13]. So

56   far, most studies on the impact and transfer of Ag-NPs in plants have been done using pristine Ag-

57   NPs. Recent opinions in nanoecotoxicology point the need of using environmentally realistic

58   experimental conditions[11], including the use of low doses (micromolar range or lower)[11] and the

59   study of aged NPs, i.e., Ag_2S-NPs. With only three published studies, data on transfer of Ag_2S-NPs in

60   plants and possible phytotoxicity is extremely scarce[14-16]. In a recent work, Wang et al. (2017) have

61   found that Ag$_2$S-NPs reduce the growth of cucumber and wheat plants, a process that seems to be

62   related with an interference with the ethylene signaling pathway, the plant defense system and

63   upward water transport[16].

64   This study aimed at clarifying the changes in speciation of Ag-NPs and Ag$_2$S-NPs in wheat and the

65   uptake and transfer pathways, and at evaluating the phytotoxic impacts in light of Ag distribution and

66   speciation. Wheat, a cereal used worldwide for food supply, was exposed to low doses, and a multi-

67   technique and multi-scale approach was applied combining X-ray micro and nano-computed

68   tomography (μ and nano-CT), micro X-ray fluorescence (μ-XRF) and micro X-ray absorption

69   spectroscopy (μ-XANES), toxicity markers and gene expression.

70

71   **2. MATHERIALS AND METHODS**

72   **2.1 Nanoparticles and chemicals**

73   Metallic silver nanoparticles (Ag-NPs) were provided by NanoAmor, Nanostructured and Amorphous

74   Materials Inc. (USA). Ag$_2$S nanoparticles (Ag$_2$S-NPs) were produced by the sulfidation of the Ag-NPs as

75   stated in Levard et al. (2011)[17] (detailed information is given in SI).

76   Pristine and sulfidized nanoparticles (Ag-NPs and Ag$_2$S NPs) were thoroughly characterized in powder

77   and in suspension (additional information is provided in SI). AgNO$_3$ powder was provided by Sigma-

78   Aldrich

79

80

81

82

83   **2.2 Plant culture**

84   Wheat (*Triticum aestivum* L.) plants were grown in hydroponics as described in SI. They were

85   randomly selected to be treated as follow follow: i) control, no Ag addition; ii) 30 µM Ag-NP; iii) 30

86   µM Ag_2S-NPs and 4) 30 µM $AgNO_3$.

87   Plants were harvested after 3 weeks of treatment. Roots and shoots were separated and thoroughly

88   rinsed with ultrapure water and Ethylenediaminetetraacetic acid (EDTA) 20mM and fresh weights

89   were recorded. Samples for phtytotoxicity studies were immediately frozen in liquid nitrogen and

90   stored at -80°C until analysis. Samples for synchrotron analysis and for X-ray computed-tomography

91   were keep fresh until specific sample preparation.

92

93   **2.3 Silver distribution and speciation in roots cross sections (synchrotron µ-XRF and µ-XANES)**

94   Fresh roots were prepared for synchrotron analyses in cryogenic conditions as stated in Larue et al.

95   (2016) [18]. µ-XRF and Ag L_{III}-edge µ-XANES measurements were performed on root thin cross sections

96   (20-30 µm) on the scanning X-ray microscope at ID21 beamline of the ESRF under cryo-conditions

97   using a vibration-free cryo-stage, passively cooled by a liquid nitrogen dewar. Detectors included a

98   Si_3N_7 diode for I_0 and a Silicon Drift Detector (X-flash Bruker 80mm^2 active area) for the emitted X-ray

99   fluorescence. Focusing was realized using Kirkpatrick-Baez mirrors system. The photon flux was

100   3.07×10^{10} ph·s^{-1} at 3.45 keV with a beam size of 0.4 x 0.6 µm. µ-XRF maps were recorded with various

101   step sizes (from 0.3 x 0.3 µm² to 4 x 4 µm²) with an incident energy of 3.45 keV, and a dwell time of

102   100 ms. Elemental maps presented in this paper were obtained after fitting each pixel XRF spectrum

103   using PyMCA software[19] as described in Castillo-Michel et al. (2016)[20].

104   In the areas of interest identified in the µ-XRF maps, Ag L_{III}-edge µ-XANES spectra were recorded by

105   single point acquisition method (3.33 to 3.45 keV energy range, 0.5 eV step). When Ag aggregates

106   were too small, the drift of the beam during acquisition did not allow to collect clean spectra. In

107   these areas, μ-XANES mapping was applied. In this case, regions of interest of 3-3.5 μm x 4.5-5 μm

108   were scanned with a step size of 0.5 μm at different energies across the Ag L_{III}-edge. Maps were

109   recorded in fluorescence mode in energy steps of 3eV from 3.32 to 3.34 keV; 0.5 eV from 3.34 to

110   3.38 and 1eV from 3.34 to 3.40 keV. A stack of the obtained 107 XANES maps was performed with

111   MATLAB routines (R2016, version 9.0) in order to get a μ-XANES spectra for each 0.5x0.5 μm^2 pixel of

112   the examined area. μ-XANES spectra were extracted by PyMCA software[19]. The possibility of

113   averaging all the μ-XANES spectra collected in the scanned area enables to get a good quality XANES

114   spectra of small NP aggregates.

115   Bulk XANES spectra of reference compounds were recorded on unfocused mode during previous

116   experiments [21] in the same conditions as samples. Ag solid state reference compounds include Ag^0

117   foil, Ag^0 nanoparticles (Ag-NPs), Ag chloride (AgCl), Ag nitrate (AgNO$_3$), Ag phosphate (Ag$_3$PO$_4$) and Ag

118   carbonate (Ag$_2$CO$_3$). Solution samples include Ag-malate (10 mM AgNO$_3$ and 100 mM malate, pH 5.5)

119   and Ag-GSH (10 mM AgNO$_3$ and 100 mM GSH, pH 5.5, prepared in anoxia). 30% glycerol was added

120   to the solutions to avoid formation of ice crystals. Additionally, the spectra of the solid state Ag$_2$S-

121   NPs and of Ag diethyldithiocarbamate (C$_5$H$_{10}$AgNS$_2$, Ag-DEDTC) were recorded for this experiment.

122   μ-XANES and XANES spectra were treated by using ATHENA software[22]. Principal components

123   Analysis (PCA) and Target Transformations (TT) were used to identify the main Ag species preset in

124   the samples. Then, their proportion in the samples was determined by Least-Squares Combination

125   Fitting (LCF) of the experimental spectra. Details about these analysis are provided in SI.

126   **2.4 Silver concentrations**

127   Immediately after harvest, shoots and roots were separated, fresh weights were recorded and they

128   were frozen in liquid N$_2$ and lyophilized. After acid digestion Ag concentrations were determined by

129   Inductively Coupled Plasma Mass Spectrometry ICP-MS (Elan DRC II Perkin Elmer). Further details are

130   provided in SI.

131

132   **2.5. 3D distribution of Ag-NPs in the roots using multi-scale X-ray computed-tomography (coupled**

133   **µ and nano-CT)**

134   Before 3D imaging, fresh roots were soaked in successive ethanol solutions (from 30% to 100% vol)

135   and dehydrated by critical point drying consisting in the replacement of ethanol by CO_2 in the

136   supercriticial state[20] .

137   3D imaging at the micro-scale (µ-CT) was performed with a Micro XCT-400 X-ray microscope (Zeiss

138   XRadia) using various magnification achieving an isotropic voxel size from 2.9 to 0.62 µm in a field of

139   view of 1024x1024x1024 voxels (3D pixels). Scans were acquired at 40 kV and 250 µA. Between 1601

140   and 2501 projections were collected with an exposure time ranging from 4s to 10s per projection

141   (depending on the magnification) through a 360° rotation.

142   The roots were also scanned in 3D at the nano-scale using an UltraXRM-L200 3D X-ray microscope

143   (Zeiss Xradia) equipped with a copper X-ray source (rotating anode) producing a polychromatic beam

144   with a maximum intensity at energy of 8.048 keV (Cu Kα-X ray emission) and Fresnel zone plate

145   providing a spatial resolution of 150 nm. Scans were recorded phase contrast mode with 901

146   projections from −90 to 90° with an angle step of 0.2° and an exposure time of 60 s per projection

147   giving a total scanning time of 17 h. The field of view (FOV) was 65x65x65 μm^3 with an isotropic voxel

148   of 63.5 nm. The FOV position of the nano-CT scan was centered at region of interest previously

149   identified by µ-CT. Reconstruction of the 3D images was performed using a Zeiss XRadia software

150   (XM Reconstructed-Parallel beam-9.0.6445 software) based on a filtered back projection algorithm.

151   Avizo 8.0 software was used for reconstructed dataset visualization.

152

153   As X-ray computed-tomography did not provide direct chemical and speciation information, 2D

154   chemical mapping was performed on the same sample. The goal was to validate the identification of

155   the Ag distribution in the samples by µ-CT and nano-CT. µ-XRF maps of the same roots and the same

7

156   regions were recorded on ID21 as described above. In this case, measurements were not performed

157   in cryogenic conditions and the photon flux was 3.1×10^{10} ph·s^{-1} at 3.45 keV.

158

159   **2.6 Phytotoxicity**

160   **2.6.1 Estimation of lipid peroxidation: malondialdehyde (MDA).**

161   Lipid peroxidation was evaluated on fresh tissues by the quantification of thiobarbituric acid reactive

162   species (TBARS) by a modified method of Reilly and Aust as stated in Pradas del Real. (2014)[23].

163   Additional information is provided in SI.

164

165   **2.6.2. Real-time polymerase chain reaction (RT-qPCR)**

166   Silver and other metals have been reported to impact the expression of genes involved in oxidative

167   stress response, defense against pathogens, metal homeostasis, salt stress and plant growth[24-26].

168   Quantitative analysis of the gene expression of selected genes was performed by reverse-

169   transcription real time PCR (RT-qPCR). Studied genes were selected to screen the potential

170   interference of NPs with main plant vital processes: oxidative balance (catalase, iron superoxidose

171   dismutase, glutathione peroxidase), homeostasis (Phosphoethanolamine N-methyltransferase),

172   pathogen defense (Pathogen-inducible ethylene-responsive element-binding protein) and growth

173   (ETTIN-like auxin response factor). The expression of the Metallothionein-like protein was also

174   studied to shed light on NPs transport processes. Target-specific PCR primers for these genes were

175   designed using Primer-BLAST[27]. Encoded genes names, accession number in NCBI database (National

176   Center for Biotechnology: https://www.ncbi.nlm.nih.gov/) and the list of primers used are given in

177   table S1.

178   RNA was isolated from plant roots by using RNeasy Plant Mini Kit (Qiagen) according to

179   manufacturer's instructions. RNA concentration and purity were assessed using a Nanodrop ND-1000

180   spectrophotometer (Thermo Fisher Scientific) by measuring absorbance at 230, 260 and 280 nm.

181   RNA was reverse transcribed into cDNA using the SuperScript II Reverse first strand kit (Invitrogen).

182   Quantitative PCR was performed in a MX3005P multiplex quantitative PCR system (Stratagene) using

183   MESA Blue qPCR Mastermix for SYBR Assay Low ROX (Eurogentec). We used the following thermal

184   cycling steps: 95°C for 5 min, then 95°C for 15 s, 55°C for 20 s and 72°C for 40 s 40 times and finally

185   95°C for 1 min, 55°C for 30 s and 95°C for 30 s for the dissociation curve. PCR efficiencies were

186   experimentally checked for compliance using a mix of all samples, with a quality criterion of 2 ± 0.3,

187   and a theoretical value of 2 was used for calculations. Actin, 18sR and GAPDHR were chosen as

188   housekeeping genes for normalization. Cq threshold was determined using the Mx-Pro 3.20 software

189   (Stratagene) with default settings. mRNA expression analysis, normalization and statistical analysis

190   were performed using the ΔΔCq method as described previously[9]. The RNA level modulation of

191   selected genes was analyzed based on Ct comparison using REST 2009 (Qiagen). Data are expressed

192   as percentages of the corresponding control ± standard deviation.

193

194   **3.   RESULTS AND DISCUSSION**

195   **3.1 Effect of initial Ag form on distribution and speciation within roots**

196   Distribution and speciation of Ag in roots were obtained by combining several highly complementary

197   imaging tools (i.e. μ-CT, nano-CT, μ-XRF and μ-XANES). μ-CT provides the in-situ 3D distribution of

198   dense voxels in intact samples and in relatively large field-of-views (FOV). Virtual cross-sections

199   (various orientation or thickness) can be extracted from the obtained reconstructed volume.

200   However, μ-CT does not provide elemental information, to validate that dense voxels can be

201   attributed to Ag accumulation regions, μ-XRF mapping of the same FOV was performed. The good

202   similarity in Ag-rich pixels (red pixels in Figure 1b or purple pixels in Figure 5b when Ag is co-localized

203   with S) and dense voxels (brilliant voxels in Figure 1a and 5a) distribution contributes to validate the

204   identification of Ag accumulation regions. μ-CT is sensitive to accumulation regions with high local Ag

205   concentration (i.e. such as Ag-NPs aggregates). However, it does not allow to discriminate Ag when it

206   is homogeneously distributed in the plant matrix (i.e. single Ag-NPs or released Ag+). Recent

207   technical developments allow performing 3D imaging with nanometer spatial resolution using X-ray

208   laboratory sources (nano-CT). Coupling μ-CT (spatial resolution at micrometer scale and relatively

209   large FOV) with nano-CT (spatial resolution of 150 nm and small FOV) offers the opportunity to

210   further study the Ag internalization processes. Synchrotron-based μ-XRF provides 2D elemental

211   information with high-sensitivity (low femtogram/μm^2)[20] and can be coupled (as in this study) to μ-

212   XANES spectroscopy to obtain speciation information.

213   The surface of plant roots exposed to $AgNO_3$ (Ag^+) contained localized accumulation zones as shown

214   by μ-CT (Figure 1a and 1b, animations 1 and 2 in supporting information). These accumulation zones

215   were not present in the control root (Figure S4.a and S5.a in SI). The 3D reconstructed image (Figure

216   1a) and the virtual cross sections (Figure 1b and animation 2 in SI) showed that these accumulation

217   zones had a variety of sizes (a few tens to 100 μm in diameter). In contrast, μ-XRF revealed an

218   homogenous presence of Ag in root epidermal cells (Figure 1.b d). μ-XRF analyses also revealed the

219   presence of Ag in the cytoplasm of cortex cells, in the endodermis and in the central cylinder (Figure

220   S2 in SI). Ag was also detected in intercellular spaces of the cortex, in accumulation regions of several

221   microns in diameter (Figure 1.e).

222   The speciation of Ag at the cortex region was determined by μ-XANES spectroscopy. In spot 1, Ag was

223   bound to thiol (84%) and O ligands (modelled by $AgNO_3$) (16%) ($AgNO_3$-cortex 1 in Figure 2).

224   Chelation by thiol ligands is a well-known detoxification mechanism inside cells, but thiol ligands are

225   also present in the apoplast[28-29]. Given the high affinity of Ag(I) for thiols, the formation of Ag-thiols

226   in the extracellular compartment is not surprising. In spot 2, a slight oscillation on the spectra at

227   3670-3380 eV was indicative of the presence of metallic Ag as minor species. Thus, part of Ag(I) was

10

228   reduced into Ag(0). The reduction of ionic Ag into Ag-NPs in plants exposed to $AgNO_3$ has been

229   reported previously[30-31], and proposed as a green technology for the production of Ag-NPs[17]. In

230   parallel, a significant Ag translocation from roots to shoots was measured (Figure S3.a). The presence

231   of Ag both in the apo-and symplast and in the central cylinder suggests that both types of transport

232   pathways, apo- and symplastic, are used by Ag ions.

233

234   For roots exposed to Ag-NPs, μ-CT and μ-XRF show the presence of localized Ag accumulation regions

235   with a size of 1-4 μm adhering on the epidermis (Figure 4.a, d, e). Metallic Ag was the major Ag

236   species of these accumulation regions (Figure. 2, root 3; Figure S4.e-f in SI, 80% and 97%

237   respectively). At higher spatial resolution, nano-CT revealed that these Ag-NPs accumulated

238   preferentially in discontinuities between root epidermal cells (Figure S5.b, c). In addition, root

239   architecture and morphology were impacted since an absence of secondary roots and a proliferation

240   of root hairs were observed exclusively for this treatment (Figure S5.a). Many Ag-NPs were fixed on

241   root hairs (Figure 4. a, Animations 3 and 4 in supporting information, Figures S6.b and S7.b in SI).

242   A higher Ag root and shoot content was observed for this treatment compared to the $AgNO_3$

243   treatment (Figure. S3), suggesting a nano-specific accumulation mechanism different to what was

244   observed for the $AgNO_3$ exposure. Our observations support two points of entry previously

245   suggested in the literature. On one hand, high local concentration of metals in the epidermis was

246   shown to cause rupture of this tissue[32]. Such ruptures in which Ag-NPs are preferentially

247   accumulated (Figure S4.b, c) might facilitate the transfer of Ag inside roots. On the other hand, root

248   hairs which have a thin cell wall, and take up nutrients by transport, diffusion, and endocytosis[33] are

249   considered as potential points of entry of NPs[12].

250   In the epidermis Ag was mostly present as metallic Ag (root 3, Figure S4 in SI). However, a

251   biotransformation of Ag was evidenced inside the roots where Ag was homogeneously distributed in

252   the cell walls of the cortex (purple areas in Figure 4.d), as a mixture of Ag-thiol species and other

253   ionic Ag species (86 and 14% respectively, Figure S2, f). Contrary to what was observed in the

254   epidermis, no Ag(0) was observed inside roots. Similar speciation results were observed in the cell

255   walls of the endodermis (77 and 26% respectively, Figure 4.c). Thus, Ag-NPs were completely

256   dissolved and complexed by organic ligands. Ag was detected inside cells of the cortex, in the

257   endodermis and in the central cylinder. These observations suggest both apoplastic and symplastic

258   transfer of Ag in monovalent form.

259

260   In the case of roots treated with Ag_2S-NPs, μ-XRF shows that Ag is mainly colocalized with S (purple

261   pixels in Figure 5b, resulting in mixing blue (S) and red (Ag)). μ-CT and nano-CT reveals that these Ag

262   accumulation regions, with a size from 3 to 8 μm are mostly on the root surface (Figure 5.a, c, b and

263   3D animations 5 and 6 in SI). μ-XANES showed that Ag at root surface was mainly present as Ag_2S,

264   with proportions ranging from 62% to 89% depending on the sample (Figure 2). Secondary Ag

265   chemical forms were also identified, including metallic Ag (up to 40%, arrows in Figure 5e). In the

266   secondary root (figure S4 in SI), no metallic Ag was found, but 13% (point 2-2) to 26% (point 2-1) of

267   Ag was bound to thiols. These results provide evidence that Ag_2S-NPs were dissolved, and then Ag+

268   ions were either complexed to thiol containing molecules or reduced to elemental Ag. These results

269   contradict the general idea that Ag_2S is highly insoluble, which is based on the solubility constant of

270   macrocrystalline Ag_2S (Ksp= $5.92 \cdot 10^{-51}$ [34]). The partial dissolution of Ag_2S could be favored by the root

271   exudation[35]. Wheat plants exudate organic acids and phytosiderophores, this process is enhanced in

272   case of nutrient deficiency or metal stress[36-38]. In a recent study with Alfalfa plants exposed to Ag_2S-

273   NPs, the authors suggested that Ag_2S could be partially dissolved in the acidic environment of root

274   border cells[15]. However, to our knowledge, this is the first work that clearly shows this process. Plants

275   and plant extracts have been used to reduce Ag(I) to Ag(0) for the green synthesis of Ag-NPs[39],

276   however this is the first time that the reduction of Ag_2S-NPs is observed in the rhizosphere

277　　(endorhizosphere and rhizoplane in this case) of living plants. The identification of the reducing agent

278　　would require further investigations.

279　　μ-XRF together with μ-CT showed that Ag_2S-NPs were especially concentrated at the base of the

280　　lateral roots (Figure 5.a,d). During the development of lateral roots, the newly formed root breaks

281　　through the cortex and endodermis. Some authors suggest that this zone may provide a direct access

282　　for NPs to the xylem[40]. Nano-CT analysis were also performed in the base of lateral roots (data not

283　　shown), however the high disorder of cell layers made impossible the clear discrimination of internal

284　　and surface areas. A few Ag-rich spots were detected inside the root only by μ-XRF (Figure 5.e, red

285　　arrows). Except these few internal Ag_2S-rich spots, very low Ag signal was detected in the cell walls

286　　and cytoplasm of the cells by μ-XRF (Figure S2 in SI) and no signal was detected in the endodermis

287　　and the central cylinder. This result is consistent with the low Ag root and shoot content measured

288　　for this treatment (Figure S3.a). Thus, despite a partial dissolution of Ag_2S-NPs near roots, Ag transfer

289　　remained limited at the present exposition time.

290

291　　**3.2. Phytotoxicity and gene expression response**

292　　Both Ag uptake in roots and translocation in shoots increased in the order Ag_2S-NP < $AgNO_3$ < Ag-NPs

293　　exposure (Figure S3.a). Plant growth reduction was correlated with Ag accumulation in tissues with

294　　the highest effect observed in the Ag-NPs treatment (Figure S3. b). However, finer phytotoxicity

295　　markers and impacts on gene expression were specific for each Ag source. Previous studies showed

296　　that the phytotoxicity of Ag-NPs was associated with reactive oxygen species production and lipid

297　　peroxidation[13]. However, no information is available about plants exposed to Ag_2S-NPs. Lipid

298　　peroxidation was evaluated by the quantification of thiobarbituric acid reactive substances (TBARS)

299　　(figure S3, c). It was the highest for the $AgNO_3$ treatment, likely due to the high concentration in Ag^+.

300　　Surprisingly, lipid peroxidation for the Ag-NPs and Ag_2S-NPs treatments was lower than the control it

301　　was thus not correlated with growth reduction.

13

302   As mentioned above, root architecture was impacted in the Ag-NPs treatment. Secondary roots did

303   not develop and a proliferation of roots hairs was observed. The presence of Ag-NPs aggregates on

304   root hairs might have an impact on their functions. Previous studies showed a loss or absence of root

305   hairs for plants exposed to Ag-NPs, but this effect may be due to the high dose used[12]. Root hair

306   proliferation is generally related with nutrient or water deficiency. The presence of Ag in the cell wall,

307   as observed in our study (Figure 4.c, d), has been suggested to affect the function of nutrient

308   transporter proteins [13]. In parallel, exposure to Ag_2S-NPs and $AgNO_3$ has been shown to down

309   regulate the expression of aquaporins[16]. Exposure to Ag-NPs was not tested in this latter study so it

310   could be related to root hair proliferation. Finally, changes in root architecture and morphology, are

311   very likely to influence the entry of Ag in nanoparticulate and ionic form.

312   In order to further investigate the phytotoxicity induced by the different sources of Ag, the

313   expression of selected genes in the roots of wheat plants was studied by real-time polymerase chain

314   reaction (RT-qPCR) (Figure 3). The genes encoding the enzymes catalase (CAT), superoxide dismutase

315   (FeSOD) and glutathione peroxidase (GPX) were studied because of their key role in the oxidative

316   stress. Each NP treatment induced changes in the expression of different genes. Ag_2S-NPs lead to the

317   overexpression of CAT and FeSOD whereas Ag-NPs induced a drop in the expression of FeSOD but an

318   increase in that of GPX. Previous studies found up-regulated expression of CAT and SOD in *Vigna*

319   *radiata*[24] and *Arabidopsis thaliana*[25-26] exposed to pristine Ag-NPs. Taken together with the TBARS

320   results and the localization and speciation of Ag, our results suggest that plants exposed to Ag-NPs

321   and Ag_2S-NPs are able to control the oxidative stress by upregulating the enzymes related with

322   radical scavenging, possibly due to the slow release of Ag^+ from the nanoparticles. Exposure to

323   $AgNO_3$, which induced a strong lipid peroxidation, did not induce any modulation of the expression of

324   these genes. A possible explanation could be that the oxidative stress exceeds to capability of the

325   enzymatic machinery, which is then not induced.

326   We investigated the expression of the gene encoding metallothionein (Wali). Metallothioneins (MTs)

327   regulate metal homeostasis, and are also involved in the scavenging of reactive oxygen species

328   (ROS)[41]. Literature regarding the production of MT's in plants exposed to Ag is scarce, with only one

329   publication reporting the overexpression of MT in wheat plants exposed to Ag^+ and Ag-NPs[9]. In the

330   present study, however, we found overexpression of Wali for $AgNO_3$ and Ag_2S-NPs treatments while

331   it was moderately but significantly down-regulated for the Ag-NPs treatment. It is suggested that the

332   synthesis of MTs in plants could be related with the detoxification of sulfide (HS-), which is

333   phytotoxic, although it has not been clearly demonstrated yet[42].   Since the speciation study

334   evidenced some dissolution of Ag_2S-NPs, the overexpression of MT found for the Ag_2S-NPs treatment

335   may be a response to a release of Ag+, but also of sulfide.

336   The three treatments also induced a down-regulation of the Phosphoethanolamine N-

337   methyltransferase (PEAMT), encoding a protein related with the salt stress, and an up-regulation of

338   the Pathogen-inducible ethylene-responsive element-binding protein (PIEP), encoding a protein

339   involved in the response to pathogens. Both results are opposite to that found for genes with similar

340   functions in a previous study with *A. thaliana*[25].

341   We also investigated the effect of the different treatments in the auxin-like response factor (ETT1).

342   Auxins are hormones that control cell proliferation and growth in plants, and are involved in root

343   branching. A crosstalk between ROS and auxin production in plant response to metal stress has been

344   evidenced[43]. In the present work, we did find an overexpression of the EET1 in the roots of $AgNO_3$

345   treated plants but no impacts were found for the two NP treatments. Thus, the absence of root

346   branching in the Ag-NPs treatment is not related to the expression of this gene.

347

348   **4.   ENVIRONMENTAL IMPLICATIONS**

349   It has been generally hypothesized that Ag-NPs may act as "Trojan Horses" entering living organisms

350   and then releasing Ag^+ over time causing toxicity[44]. This has been recently proposed as the

15

351   mechanism by which Ag₂S-NPs could be toxic to wheat and cowpea. In the present work, although

352   the Trojan horse scenario is very likely to take place, a more complex scheme was evidenced. As

353   illustrated in the synthetic Figure 6, interconversions of Ag forms outside and inside the plant,

354   leading to a mixture of Ag species, were observed. The distribution of Ag species probably evolves

355   over time, leading to a complex exposition pattern for plants, also exposed to HS⁻ in the case of Ag₂S-

356   NPs. The conflicting results usually seen in the literature concerning the toxicity of silver

357   nanoparticles are generally ascribed to differences in exposure conditions, structural properties of

358   nanoparticles and plant species. This evolving Ag speciation may represent an additional source of

359   variability and conflicting results.

360

361   Data from this study showed drastic different responses of the plant depending on the starting

362   nanoparticles, highlighting the importance to include transformed nanoparticles in ecotoxicological

363   studies.

364   Although the uptake and translocation of Ag was lower for the Ag₂S-NPs exposure compared to the

365   Ag-NPs exposure, phytotoxicity symptoms were observed. These results show that the sulfidation of

366   Ag-NPs is not a perfect antidote to toxicity and that Ag₂S-NPs are not as stable as expected when

367   exposed to plant roots. In agricultural soils, the rhizospheric activity of plants might partly dissolve

368   Ag₂S causing some impacts on crop quality and yield, and more generally on ecological services.

369

374   equipments available for the project. ISTerre is also part of Labex OSUG@2020 (ANR10 LABX56).We

375   thank the ESRF for providing PRC and "in house" beam time.

376

377

378

379

380   **REFERENCES**

381

382   1.   Gottschalk, F.; Sonderer, T.; Scholz, R. W.; Nowack, B., Modeled environmental
383   concentrations of engineered nanomaterials (TiO$_2$, ZnO, Ag, CNT, fullerenes) for different regions.
384   *Environ. Sci. Technol.* **2009,** *43*, 9216-9222.
385   2.   Pradas del Real, A. E.; Castillo-Michel, H. A.; Kaegi, R.; Sinnet, B.; Magnin, V.; Findling, N.;
386   Villanova, J.; Carriere, M.; Santaella, C.; Fernandez-Martinez, A., Fate of Ag-NPs in sewage sludge
387   after application on agricultural soils. *Environ. Sci. Technol.* **2016**.
388   3.   Kah, M.; Hofmann, T., Nanopesticide research: current trends and future priorities.
389   *Environment International* **2014,** *63*, 224-235.
390   4.   Ma, X. M.; Geiser-Lee, J.; Deng, Y.; Kolmakov, A., Interactions between engineered
391   nanoparticles (ENPs) and plants: Phytotoxicity, uptake and accumulation. *Sci. Total Environ.* **2010,**
392   *408* (16), 3053-3061.
393   5.   Gottschalk, F.; Nowack, B., The release of engineered nanomaterials to the environment.
394   *Journal of Environmental Monitoring* **2011,** *13* (5), 1145-1155.
395   6.   Levard, C.; Hotze, E. M.; Colman, B. P.; Dale, A. L.; Truong, L.; Yang, X. Y.; Bone, A. J.; Brown,
396   G. E.; Tanguay, R. L.; Di Giulio, R. T.; Bernhardt, E. S.; Meyer, J. N.; Wiesner, M. R.; Lowry, G. V.,
397   Sulfidation of Silver Nanoparticles: Natural Antidote to Their Toxicity. *Environ. Sci. Technol.* **2013,** *47*
398   (23), 13440-13448.
399   7.   Li, L.; Wang, Y.; Liu, Q.; Jiang, G., Rethinking Stability of Silver Sulfide Nanoparticles (Ag2S-
400   NPs) in the Aquatic Environment: Photoinduced Transformation of Ag2S-NPs in the Presence of Fe
401   (III). *Environ. Sci. Technol.* **2015,** *50* (1), 188-196.
402   8.   Anjum, N. A.; Gill, S. S.; Duarte, A. C.; Pereira, E.; Ahmad, I., Silver nanoparticles in soil-plant
403   systems. *J. Nanopart. Res.* **2013,** *15* (9).
404   9.   Dimkpa, C. O.; McLean, J. E.; Martineau, N.; Britt, D. W.; Haverkamp, R.; Anderson, A. J., Silver
405   Nanoparticles Disrupt Wheat (Triticum aestivum L.) Growth in a Sand Matrix. *Environ. Sci. Technol.*
406   **2013,** *47* (2), 1082-1090.
407   10.   Gubbins, E. J.; Batty, L. C.; Lead, J. R., Phytotoxicity of silver nanoparticles to Lemna minor L.
408   *Environ. Pollut.* **2011,** *159* (6), 1551-1559.
409   11.   Holden, P. A.; Gardea-Torresdey, J.; Klaessig, F.; Turco, R. F.; Mortimer, M.; Hund-Rinke, K.;
410   Cohen Hubal, E. A.; Avery, D.; Barcelo, D.; Behra, R.; Cohen, Y.; Deydier-Stephan, L.; Ferguson, P. L.;
411   Fernandes, T. F.; Herr Harthorn, B.; Henderson, W. M.; Hoke, R. A.; Hristozov, D.; Johnston, J. M.;
412   Kane, A. B.; Kapustka, L.; Keller, A. A.; Lenihan, H. S.; Lovell, W.; Murphy, C. J.; Nisbet, R. M.; Petersen,
413   E. J.; Salinas, E. R.; Scheringer, M.; Sharma, M.; Speed, D. E.; Sultan, Y.; Westerhoff, P.; White, J. C.;
414   Wiesner, M. R.; Wong, E. M.; Xing, B.; Steele Horan, M.; Godwin, H. A.; Nel, A. E., Considerations of
415   Environmentally Relevant Test Conditions for Improved Evaluation of Ecological Hazards of
416   Engineered Nanomaterials. *Environ. Sci. Technol.* **2016**.

417 12. Schwab, F.; Zhai, G.; Kern, M.; Turner, A.; Schnoor, J. L.; Wiesner, M. R., Barriers, pathways
418 and processes for uptake, translocation and accumulation of nanomaterials in plants - Critical review.
419 *Nanotoxicology* **2016,** *10* (3), 257-278.
420 13. Zuverza-Mena, N.; Martínez-Fernández, D.; Du, W.; Hernandez-Viezcas, J. A.; Bonilla-Bird, N.;
421 López-Moreno, M. L.; Komárek, M.; Peralta-Videa, J. R.; Gardea-Torresdey, J. L., Exposure of
422 engineered nanomaterials to plants: Insights into the physiological and biochemical responses-A
423 review. *Plant Physiology and Biochemistry* **2016.**
424 14. Wang, P.; Menzies, N. W.; Lombi, E.; Sekine, R.; Blamey, F. P. C.; Hernandez-Soriano, M. C.;
425 Cheng, M.; Kappen, P.; Peijnenburg, W. J.; Tang, C., Silver sulfide nanoparticles (Ag$_2$S-NPs) are taken
426 up by plants and are phytotoxic. *Nanotoxicology* **2015,** (0), 1-9.
427 15. Stegemeier, J. P.; Schwab, F.; Colman, B. P.; Webb, S. M.; Newville, M.; Lanzirotti, A.; Winkler,
428 C.; Wiesner, M. R.; Lowry, G. V., Speciation Matters: Bioavailability of Silver and Silver Sulfide
429 Nanoparticles to Alfalfa (Medicago sativa). *Environ. Sci. Technol.* **2015,** *49* (14), 8451-8460.
430 16. Wang, P.; Lombi, E.; Sun, S.; Scheckel, K. G.; Malysheva, A.; McKenna, B. A.; Menzies, N. W.;
431 Zhao, F.-J.; Kopittke, P. M., Characterizing the uptake, accumulation and toxicity of silver sulfide
432 nanoparticles in plants. *Environmental Science: Nano* **2017.**
433 17. Levard, C.; Reinsch, B. C.; Michel, F. M.; Oumahi, C.; Lowry, G. V.; Brown, G. E., Sulfidation
434 Processes of PVP-Coated Silver Nanoparticles in Aqueous Solution: Impact on Dissolution Rate.
435 *Environ. Sci. Technol.* **2011,** *45* (12), 5260-5266.
436 18. Larue, C.; Castillo-Michel, H.; Stein, R. J.; Fayard, B.; Pouyet, E.; Villanova, J.; Magnin, V.; del
437 Real, A.-E. P.; Trcera, N.; Legros, S., Innovative combination of spectroscopic techniques to reveal
438 nanoparticle fate in a crop plant. *Spectrochimica Acta Part B: Atomic Spectroscopy* **2016,** *119*, 17-24.
439 19. Solé, V.; Papillon, E.; Cotte, M.; Walter, P.; Susini, J., A multiplatform code for the analysis of
440 energy-dispersive X-ray fluorescence spectra. *Spectrochimica Acta Part B: Atomic Spectroscopy* **2007,**
441 *62* (1), 63-68.
442 20. Castillo-Michel, H. A.; Larue, C.; del Real, A. E. P.; Cotte, M.; Sarret, G., Practical review on the
443 use of synchrotron based micro-and nano-X-ray fluorescence mapping and X-ray absorption
444 spectroscopy to investigate the interactions between plants and engineered nanomaterials. *Plant
445 Physiology and Biochemistry* **2016.**
446 21. Larue, C.; Castillo-Michel, H.; Sobanska, S.; Cecillon, L.; Bureau, S.; Barthes, V.; Ouerdane, L.;
447 Carriere, M.; Sarret, G., Foliar exposure of the crop Lactuca sativa to silver nanoparticles: Evidence
448 for internalization and changes in Ag speciation. *Journal of Hazardous Materials* **2014,** *264*, 98-106.
449 22. Ravel, B.; Newville, M., ATHENA, ARTEMIS, HEPHAESTUS: data analysis for X-ray absorption
450 spectroscopy using IFEFFIT. *Journal of Synchrotron Radiation* **2005,** *12* (4), 537-541.
451 23. Pradas del Real, A.; García-Gonzalo, P.; Lobo, M.; Pérez-Sanz, A., Chromium speciation
452 modifies root exudation in two genotypes of Silene vulgaris. *Environmental and Experimental Botany*
453 **2014,** *107*, 1-6.
454 24. Nair, P. M. G.; Chung, I. M., Physiological and molecular level studies on the toxicity of silver
455 nanoparticles in germinating seedlings of mung bean (Vigna radiata L.). *Acta Physiologiae Plantarum*
456 **2015,** *37* (1).
457 25. Kaveh, R.; Li, Y. S.; Ranjbar, S.; Tehrani, R.; Brueck, C. L.; Van Aken, B., Changes in Arabidopsis
458 thaliana Gene Expression in Response to Silver Nanoparticles and Silver Ions. *Environ. Sci. Technol.*
459 **2013,** *47* (18), 10637-10644.
460 26. Syu, Y. Y.; Hung, J. H.; Chen, J. C.; Chuang, H. W., Impacts of size and shape of silver
461 nanoparticles on Arabidopsis plant growth and gene expression. *Plant Physiology and Biochemistry*
462 **2014,** *83*, 57-64.
463 27. Ye, J.; Coulouris, G.; Zaretskaya, I.; Cutcutache, I.; Rozen, S.; Madden, T. L., Primer-BLAST: a
464 tool to design target-specific primers for polymerase chain reaction. *BMC bioinformatics* **2012,** *13* (1),
465 134.
466 28. Yang, Y.; Zhang, F.; He, W.; Wang, X.; Zhang, L., Iron-mediated inhibition of H+-ATPase in
467 plasma membrane vesicles isolated from wheat roots. *Cellular and Molecular Life Sciences CMLS*
468 **2003,** *60* (6), 1249-1257.

469 29.   Ferretti, M.; Destro, T.; Tosatto, S.; La Rocca, N.; Rascio, N.; Masi, A., Gamma-glutamyl
470 transferase in the cell wall participates in extracellular glutathione salvage from the root apoplast.
471 *New Phytologist* **2009,** *181* (1), 115-126.
472 30.   Berumen, J. P.; Gallegos-Loya, E.; Esparza-Ponce, H.; Gonzalez-Valenzuela, R.; Gonzalez-
473 Valenzuela, C.; Duarte-Moller, A., *XAS Study of silver nanoparticles formed in phaseolus vulgaris.*
474 **2009**; p 211-215.
475 31.   Gardea-Torresdey, J. L.; Gomez, E.; Peralta-Videa, J. R.; Parsons, J. G.; Troiani, H.; Jose-
476 Yacaman, M., Alfalfa sprouts: A natural source for the synthesis of silver nanoparticles. *Langmuir*
477 **2003,** *19* (4), 1357-1361.
478 32.   Wang, P.; Menzies, N. W.; Lombi, E.; McKenna, B. A.; de Jonge, M. D.; Donner, E.; Blamey, F.
479 P. C.; Ryan, C. G.; Paterson, D. J.; Howard, D. L., Quantitative determination of metal and metalloid
480 spatial distribution in hydrated and fresh roots of cowpea using synchrotron-based X-ray
481 fluorescence microscopy. *Sci. Total Environ.* **2013,** *463*, 131-139.
482 33.   Ovečka, M.; Lang, I.; Baluška, F.; Ismail, A.; Illeš, P.; Lichtscheidl, I. K., Endocytosis and vesicle
483 trafficking during tip growth of root hairs. *Protoplasma* **2005,** *226* (1-2), 39-54.
484 34.   Lide, D. R., *CRC handbook of chemistry and physics*. CRC press: **2004**.
485 35.   Hinsinger, P., Bioavailability of trace elements as related to root-induced chemical changes in
486 the rhizosphere. *Trace elements in the rhizosphere* **2001**, 25-41.
487 36.   Li, Y.; Wang, L.; Yang, L.; Li, H., Dynamics of rhizosphere properties and antioxidative
488 responses in wheat (Triticum aestivum L.) under cadmium stress. *Ecotox. Environ. Safe.* **2014,** *102*,
489 55-61.
490 37.   Nian, H.; Yang, Z. M.; Ahn, S. J.; Cheng, Z. J.; Matsumoto, H., A comparative study on the
491 aluminium- and copper-induced organic acid exudation from wheat roots. *Physiologia Plantarum*
492 **2002,** *116* (3), 328-335.
493 38.   Oburger, E.; Gruber, B.; Schindlegger, Y.; Schenkeveld, W. D.; Hann, S.; Kraemer, S. M.;
494 Wenzel, W. W.; Puschenreiter, M., Root exudation of phytosiderophores from soil-grown wheat.
495 *New Phytologist* **2014,** *203* (4), 1161-1174.
496 39.   Kumar, V.; Yadav, S. K., Plant-mediated synthesis of silver and gold nanoparticles and their
497 applications. *Journal of Chemical Technology and Biotechnology* **2009,** *84* (2), 151-157.
498 40.   Dietz, K.-J.; Herth, S., Plant nanotoxicology. *Trends in Plant Science* **2011,** *16* (11), 582-589.
499 41.   Hassinen, V. H.; Tervahauta, A. I.; Schat, H.; Karenlampi, S. O., Plant metallothioneins - metal
500 chelators with ROS scavenging activity? *Plant Biology* **2011,** *13* (2), 225-232.
501 42.   Lamers, L. P. M.; Govers, L. L.; Janssen, I. C.; Geurts, J. J.; Van der Welle, M. E.; Van Katwijk,
502 M. M.; Van der Heide, T.; Roelofs, J. G.; Smolders, A. J., Sulfide as a soil phytotoxin - A review.
503 *Frontiers in Plant Science* **2013,** *4*.
504 43.   Yuan, H.-M.; Liu, W.-C.; Jin, Y.; Lu, Y.-T., Role of ROS and auxin in plant response to metal-
505 mediated stress. *Plant signaling & behavior* **2013,** *8* (7), e24671.
506 44.   Lubick, N., Nanosilver toxicity: ions, nanoparticles or both? *Environ. Sci. Technol.* **2008,** *42*
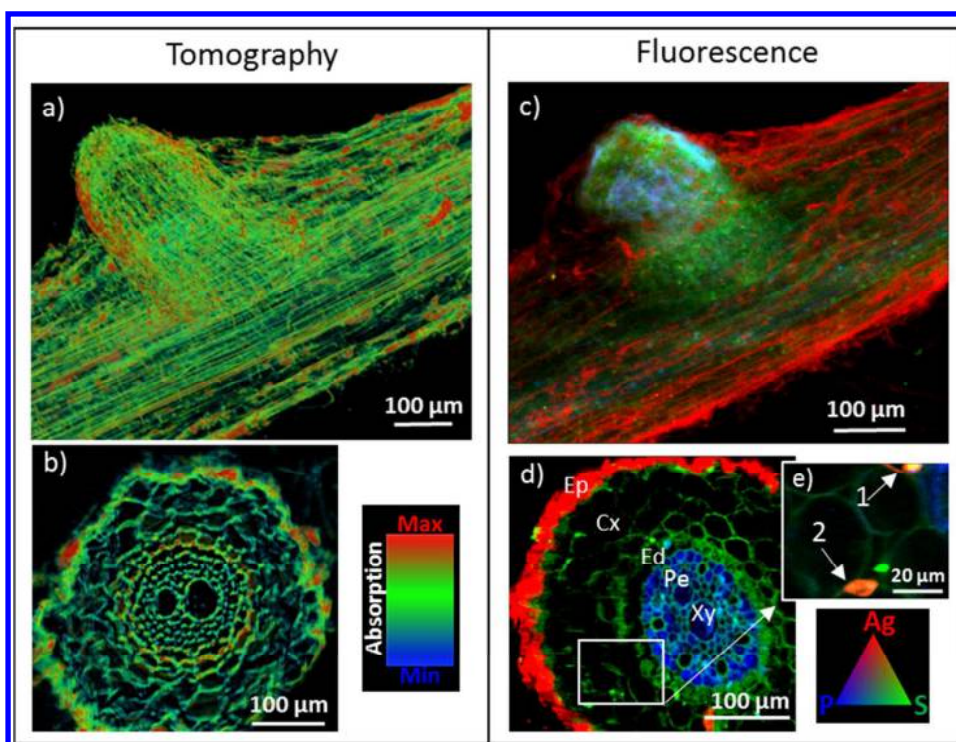507 (23), 8617-8617.

508

509

510

511

512

513

514

515

516

517

518

519

520

521

522

523

524

525   **FIGURES**

526

527

528   **Figure 1**. Roots of wheat plants exposed to $AgNO_3$: a) 3D reconstructed image by μ-CT (voxel size 1
529   μm) b) virtual 2D slice (1 μm thickness) extracted from a). μ-XRF tricolor maps of entire root (1 px = 1
530   μm) (c), of cross section (1 px = 1 μm) (Ep=epidermis, Cx=cortex, Ed= endodermis, Pe=pericycle,
531   Xy=xylem) (d) and   of a zoom in the cortex (1 px = 0.5 μm) (e). Extremity of white arrows in e)
532   indicate points where μ-XANES spectra were collected.

533

534

535

536

20

537

538
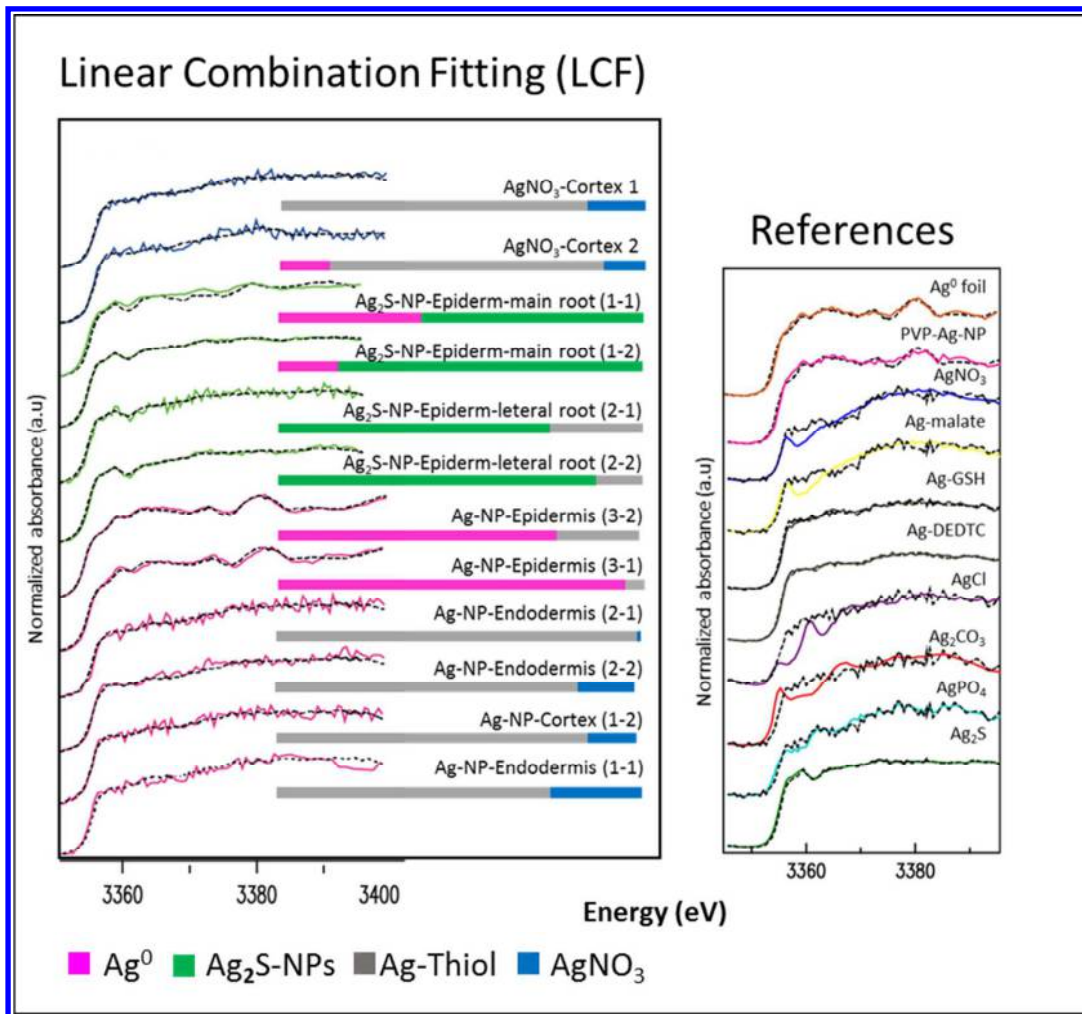
Figure 2: Linear combination Fitting (LCF) of the µ-XANES spectra collected in the different points of the samples (dotted lines), experimental spectra (soild lines). Results for the Linear Combination Fitting (LCF) of all samples are given in table S2 of SI. And Ag references used (solid lines) and reconstruction of these references by Target Transformation (dotted lines) for the three components determined by Principal Components Analysis (PCA). Reference of $AgNO_3$ is a proxy for Ag^+ species ligated to O ligands. Ag-GSH (Ag-glutathione) and Ag-DEDTC (Ag- diethyldithiocarbamate) were indistinguishable and were used as proxy of Ag-Thiol. The spectra of Ag0 foil and Ag-NPs were also indistinguishable and were used as references for metallic Ag.
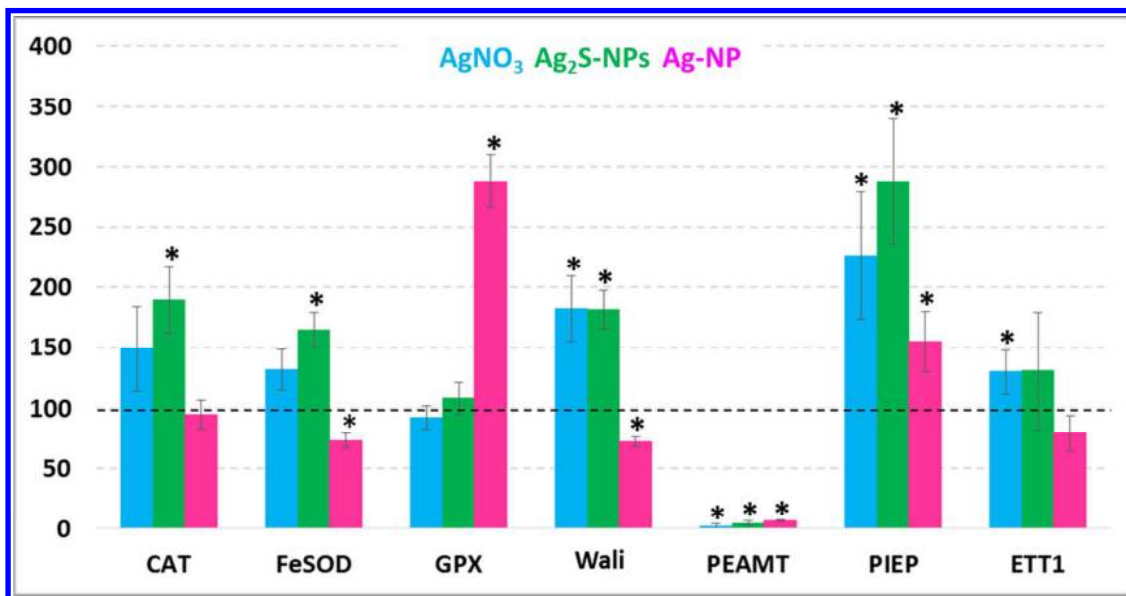
547

548

549

550

551

552

553

554

555

556

557 **Figure 3**. Gene expression quantified by qPCR in roots of plants exposed to $AgNO_3$ (blue), Ag_2S-NPs
558 (green) and Ag-NPs (pink). Results are expressed as fold change regards control. They represent the
559 average of 3 analytical replicates ± standard deviation, (*p < 0.05). CAT (catalase), FeSOD (iron
560 superoxidose dismutase), GPX (glutathione peroxidase), Wali (Metallothionein-like protein) PEAMP
561 (Phosphoethanolamine N-methyltransferase), PIEP (Pathogen-inducible ethylene-responsive
562 element-binding protein), ETT1 (ETTIN-like auxin response factor).

563

564

565

566
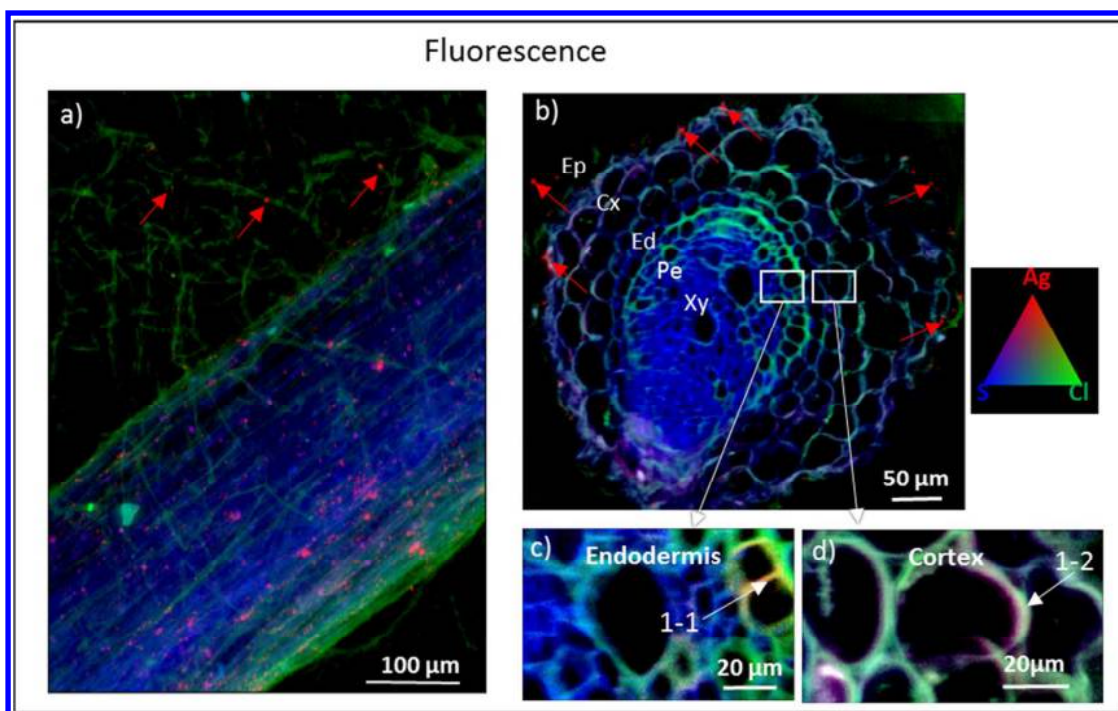
Figure 4. Roots of wheat plants exposed to Ag-NPs, μ-XRF tricolor maps of a) entire root (1 px = 1 μm) (1 px = 1 μm), (b) root cross section (Sf=surface, Ep=epidermis, Cx=cortex, Ed= endodermis, Pe=pericycle, Xy=xylem) (b), and of a zoom in the endodermis (c) and cortex (d) (1px = 0.5μm). Red arrows show preferential accumulation sites for Ag-NPs. Extremity of white arrows in c) and d) indicate points where μ-XANES spectra were collected.
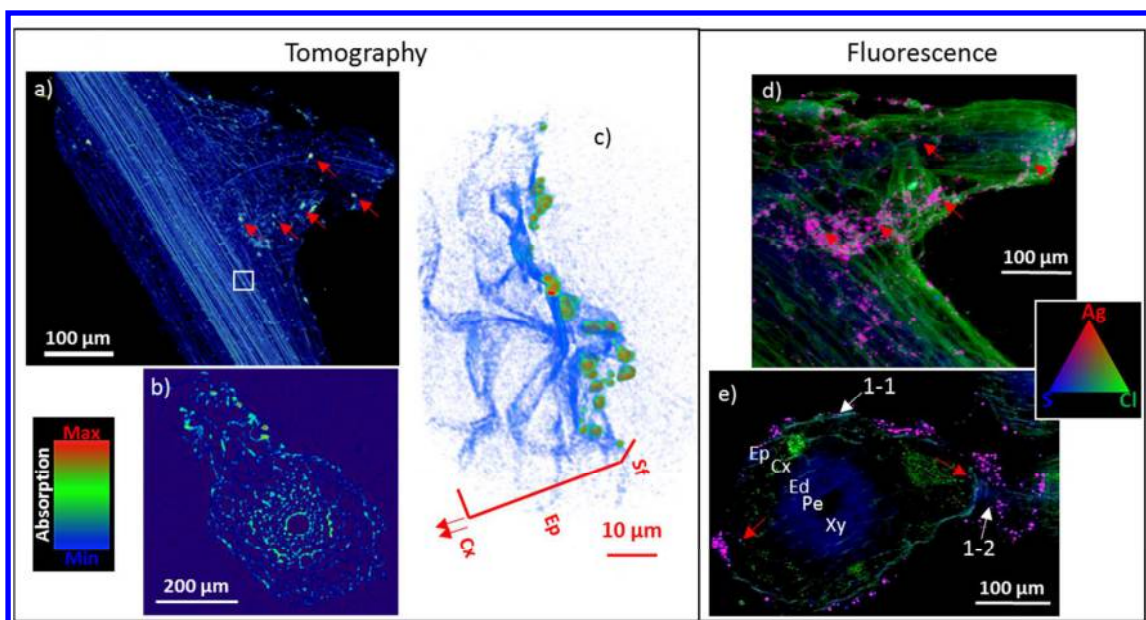
578

Figure 5. Roots of wheat plants exposed to Ag_2S-NPs: a) 3D reconstructed image by μ-CT (voxel size
0.9 μm), b) virtual μ-CT slice (1 μm thickness) extracted from a), c) nano-CT reconstructed image of
the primary root surface (white square in a)) (voxel size of 63.5 nm). μ-XRF maps of entire root (1 px
= 1 μm) d), of a cross section (e) (Sf=surface, Ep=epidermis, Cx=cortex, Ed= endodermis, Pe=pericycle,
Xy=xylem) . Red arrows indicate equivalent Ag accumulation regions in images. White arrows in e)
indicate points where μ-XANES spectra were collected.

585
586

587
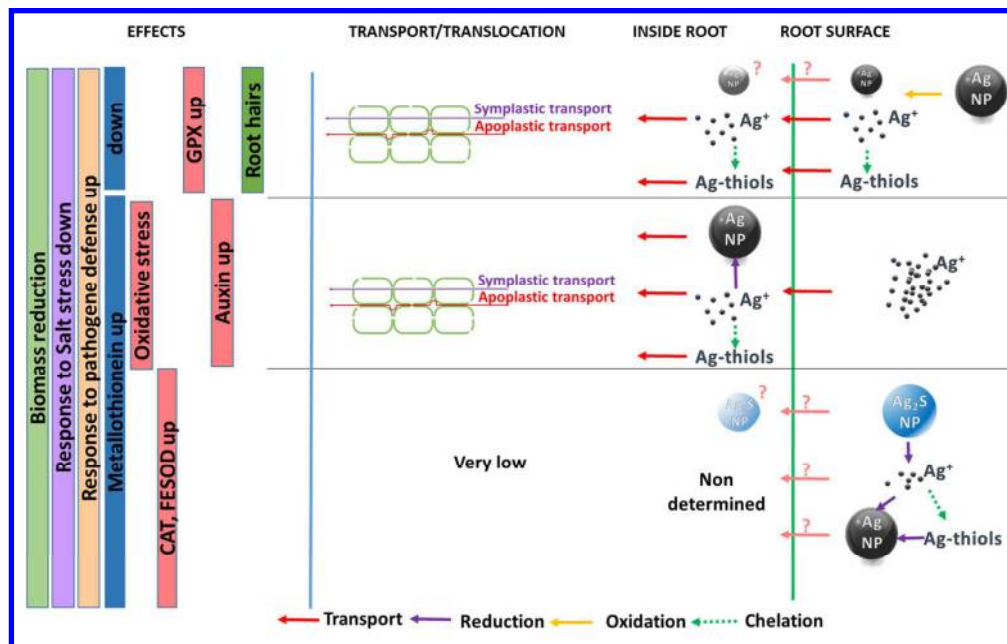
Figure 6. Synthesis of the observed changes in Ag speciation that take place inside and outside wheat
roots depending on the starting materials, proposed transfer pathways and induced effects on
plants.

591

592

24